Enhanced Photoassisted Water Electrolysis Using Vertically Oriented Anodically Fabricated Ti−Nb−Zr−O Mixed Oxide Nanotube Arrays

Nageh K. Allam,[†,§] Faisal Alamgir,[‡] and Mostafa A. El-Sayed[†,*]

[†]Laser Dynamics Laboratory, School of Chemistry and Biochemistry and [‡]School of Materials Science and Engineering, Georgia Institute of Technology, Atlanta, Georgia 30332-0400. [§]Permanent address: Electrochemistry Laboratory, National Research Center, Dokki, Cairo 12622, Egypt..

ABSTRACT Self-ordered, highly oriented arrays of titanium−niobium−zirconium mixed oxide nanotube films were fabricated by the anodization of $Ti_{35}Nb_5Zr$ alloy in aqueous and formamide electrolytes containing NH_4F at room temperature. The nanostructure topology was found to depend on the nature of the electrolyte and the applied voltage. Our results demonstrate the possibility to grow mixed oxide nanotube array films possessing several-micrometer-thick layers by a simple and straightforward electrochemical route. The fabricated Ti−Nb−Zr−O nanotubes showed a ~17.5% increase in the photoelectrochemical water oxidation efficiency as compared to that measured for pure TiO_2 nanotubes under UV illumination (100 mW/cm^2, 320−400 nm, 1 M KOH). This enhancement could be related to a combination of the effect of the thin wall of the fabricated Ti−Nb−Zr−O nanotubes (10 ± 2 nm) and the formation of Zr oxide and Nb oxide layers on the nanotube surface, which seems to slow down the electron−hole recombination in a way similar to that reported for Grätzel solar cells.

KEYWORDS: anodization · Ti−Nb−Zr−O · nanotubes · photocurrent · efficiency · water splitting

It is now generally recognized that nanoscale control of metal oxide architectures leads to the development of new materials and systems with unique physical and chemical properties. In this regard, the anodization technique is considered as an efficient and well-developed surface treatment process used in the fabrication of a variety of nanoarchitectures.[1−6] As an important n-type semiconductor material, due to their low cost, nontoxicity, stability, and vectorial charge transfer, anodically fabricated TiO_2 nanotubes have recently stimulated increasing attention because of their promising applications in many fields, including sensors, self-cleaning photocatalytic surfaces and devices, dye-sensitized solar cells, and hydrogen generation by water photoelectrolysis.[7,8] In most of these applications, the discovery of a single semiconductor material that is fully functioning is yet to come. Therefore, a common and promising approach is to develop, optimize, and employ semiconductor materials composed of 1D nanoarchitectures of mixed oxides especially for applications based on photocatalytic properties.[9,10]

In a recent work, Mor and co-workers reported on the formation of Ti−Fe−O mixed oxide nanotube arrays with enhanced photoelectrochemical water-splitting performance.[11] They related this enhancement to the combined properties of both TiO_2 and Fe_2O_3. On the basis of these promising results, they expanded the work to fabricate a p-type Ti−Cu−O nanoarchitectured electrode to construct a self-biased photodiode for water splitting.[12] Nah and co-workers were able to fabricate Ti−W−O nanotubes *via* the anodization of Ti−W alloy films containing different proportions of W.[13] The fabricated composite Ti−W−O nanotubes showed highly improved ion insertion and electrochromic properties, even when only small amounts such as 0.2 at. % WO_3 were present. Bayoumi and Ateya[14] as well as Berger and co-workers[15] reported on the fabrication of Ti−Al−O nanotubes *via* the anodization of Ti−Al alloys. Mohapatra and co-workers reported on the fabrication of 0.5−2 μm long Ti−Mn−O nanotube arrays by the anodic oxidation of Ti_8Mn for a high-capacity lithium ion battery.[16] They found that the length and diameter of the nanotubes grown on the β-phase, which contained more Mn, were smaller than those grown on the α-phase. Ghicov and co-workers reported the anodization of $Ti_{45}Nb$ to grow Ti−Nb−O nanotubes that showed enhanced thermal stability as compared to pure TiO_2 nanotube arrays.[17] Also, Ding and co-workers reported the fabrication of Ti−Nb−O nanotubes containing less Nb

*Address correspondence to melsayed@gatech.edu, nageh.allam@gmail.com.

Received for review July 18, 2010 and accepted August 31, 2010.

Published online September 3, 2010.
10.1021/nn101678n

via the anodization of $Ti_{35}Nb$ alloy.[18] Yasuda and Schmuki fabricated Ti−Zr−O nanotubes *via* the anodization of $Ti_{50}Zr$ alloy.[19]

Despite all these reports, (1) it is still a challenge to fabricate a suite of uniform nanotubular architectures of titanium mixed oxides several micrometers in length with thin-wall thicknesses that are less than the minority carrier diffusion length,[8] and (2) to the best of our knowledge, there is no report in the literature on the utilization of Ti−Nb−Zr−O nanotubes as photoanodes for photoelectrochemical water splitting, although Nb is well known to stabilize the anatase phase, which is the most photoactive polymorph of TiO_2, and both Nb_2O_5 and ZrO_2 are being used as buffer layers to improve the efficiency of Grätzel solar cells.

In this study, we report on the fabrication of a well-organized suite of Ti−Nb−Zr−O nanotube array films with very thin wall thicknesses (10 ± 2 nm) *via* the anodization of $Ti_{35}Nb_5Zr$ alloy in fluoride-containing electrolytes. Our ability to fabricate nanotubular structures of mixed/graded oxides is significant, as the nanotube array architecture allows for the precise design and control of the geometrical features, allowing one to achieve a material with specific light absorption and propagation characteristics.[8] Also, the aligned porosity, crystallinity, and oriented nature of the nanotubular structure make this architecture an attractive electron percolation pathway for vectorial charge transfer between interfaces.[7,8] On the other hand, we report here, for the first time, on the photoelectrochemical performance of these Ti−Nb−Zr−O photoanodes for photoassisted water electrolysis. We hope that this study will open a new vista to explore more combinations for a diversity of various applications.

RESULTS AND DISCUSSION

Morphological and Structural Characterization. Figure 1 shows field emission scanning electron microscopy (FESEM) top-view images of the films synthesized by anodizing $Ti_{35}Nb_5Zr$ samples in aqueous electrolytes containing 0.2 M NH_4F and 0.1 M H_3PO_4 for 7 h at different applied voltages. Anodization at 10 V, Figure 1a, resulted in the formation of a compact film with small pits scattered on some localized areas of the surface. The corresponding anodization current−time response of the sample shows a characteristic diminishment with increasing time as the oxide thickness steadily increases, with some small fluctuations in the current amplitude similar to those recorded during the initiation of pitting on metallic substrates.[8,20] Figure 1b shows the morphology of a sample anodized at 15 V. Note that the surface is completely porous, with no tubular structure observed. The

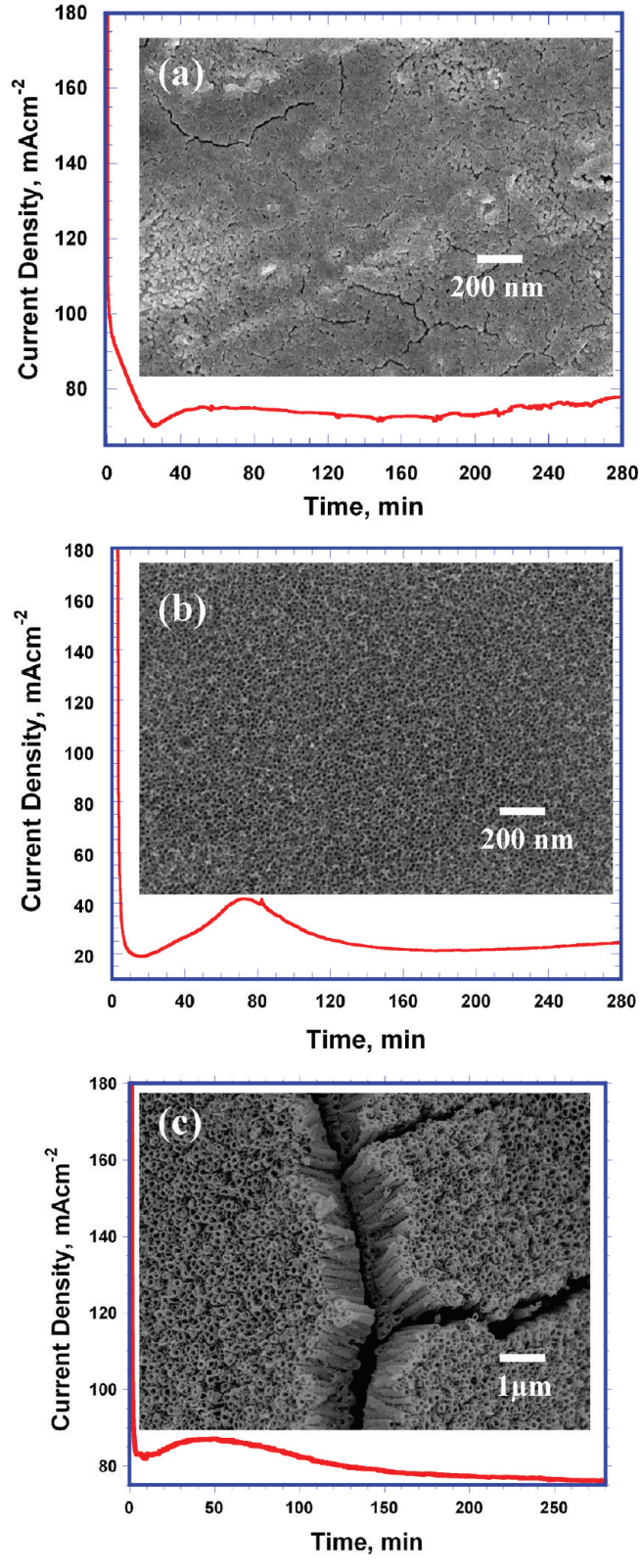

Figure 1. FESEM top-view images and the corresponding current−time relations for $Ti_{35}Nb_5Zr$ samples anodized for 7 h in aqueous electrolytes containing 0.2 M NH_4F and 0.1 M H_3PO_4 at (a) 10, (b) 15, and (c) 20 V.

corresponding current−time behavior is essentially identical to that seen when nanoporous films are achieved *via* anodization of Ti in aqueous solutions.[8] Upon increasing the applied voltage to 20 V, nanotubular arrays were obtained with irregular outer diameters of 90 ± 20 nm and lengths of 1.4 ± 0.4 μm, see Figure 1c. This is very similar to the nanotubes fabricated by the anodization of pure titanium metal in aqueous electrolytes, which are always short in length and contain ridges and circumferential serrations.[8] The corresponding current−time behavior, including the classic dip−rise−gradual fall, is essentially identical to that seen when nanotube arrays are achieved *via* anodization of Ti in fluoride-containing electrolytes.[8] It is noteworthy to mention that anodization at 20 V for shorter time intervals resulted in the formation of morphologies similar to that shown in Figure 1b. However, anodization at higher applied voltages (>20 V) resulted in complete deterioration of the Ti−Nb−Zr alloy samples.

As we were unable to fabricate long, smooth, and ridge-free nanotubular arrays in aqueous electrolytes, we aimed at anodizing the $Ti_{35}Nb_5Zr$ alloy samples in formamide-containing electrolytes. Figure 2 shows the FESEM images obtained for samples anodized in formamide-based electrolytes containing 0.2 M NH_4F, 0.1 M H_3PO_4, and 3 vol % H_2O for 20 h at different applied voltages (20−50 V). At 20 V, Figure 2a, randomly oriented nanoarchitectures were formed with a great tendency toward agglomeration forming bundles of 4 μm long nanotubes/nanowires. Increasing the anodization voltage to 30 V, Figure 2b, resulted in the formation of more organized, vertically oriented 7 μm long nanotube array films. Further increase in the applied voltage to 40 V, Figure 2c, resulted in the formation of nanoarchitectures similar to those obtained at 30 V but with apparently larger diameters. However, anodization at 50 V resulted in the formation of randomly oriented nanotubes with cracks observed on the surface. Figure 2d shows the current−time relations recorded for Ti−Nb−Zr samples anodized at 20, 30, and 40 V. The plots are typical of those obtained in the case of Ti metal anodized in similar electrolytes,[8] with the curves being similar to each other but with some minor differences in the current density values.

In order to investigate the composition of the Ti−Nb−Zr−O nanotube arrays synthesized in formamide electrolyte, we have performed X-ray photoelectron spectroscopy (XPS) analysis for the nanotubes after their annealing at 500 °C in adry oxygen atmosphere. Figure 3 shows the XPS results from a sample that was anodized in a formamide-based electrolyte containing 0.2 M NH_4F, 0.1 M H_3PO_4, and 3 vol % H_2O at 40 V. Figure 3a shows Ti 2p spectra where two peaks were obtained corresponding to Ti $2p_{3/2}$ and Ti $2p_{1/2}$ photoemission spectra with a spin−orbit splitting of 5.7 eV, confirming that both signals correspond to

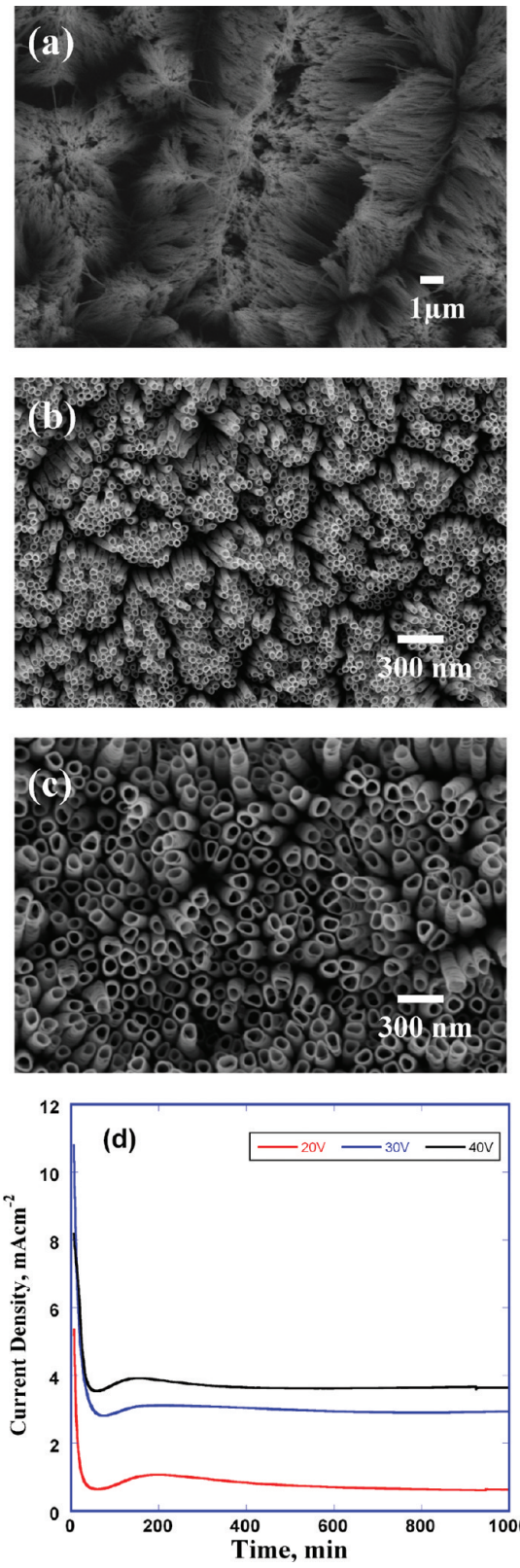

Figure 2. FESEM top-view images for $Ti_{35}Nb_5Zr$ samples anodized for 20 h in formamide electrolytes containing 0.2 M NH_4F and 0.1 M H_3PO_4 at (a) 20, (b) 30, and (c) 40 V; (d) is the corresponding current−time relations.

Ti^{4+}.[21] Figure 3b represents the Nb 3d spectra, where the peak at ~207.4 eV corresponds to the Nb $3d_{5/2}$

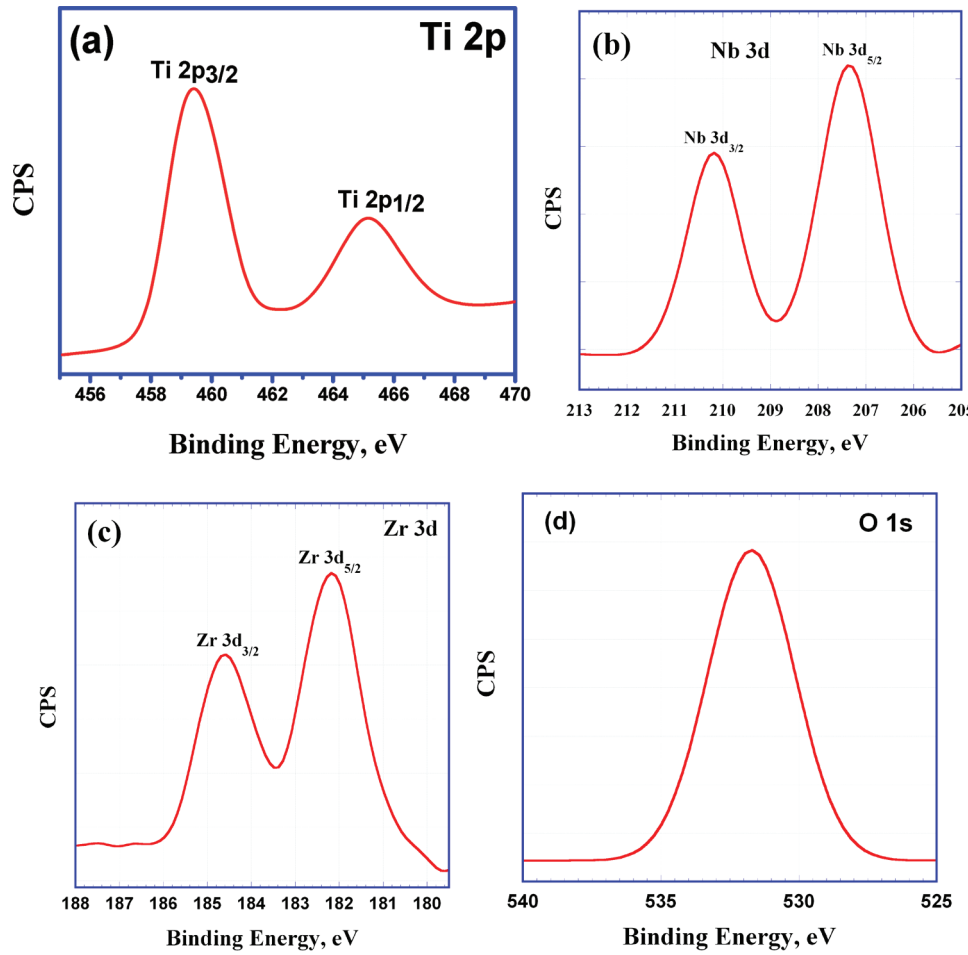

Figure 3. XPS spectra obtained for annealed Ti−Nb−Zr−O nanotubes fabricated *via* the anodization of $Ti_{35}Nb_5Zr$ alloy in a formamide electrolyte containing 0.2 M NH_4F and 0.1 M H_3PO_4 at 40 V for 20 h, see text.

while that at ~210.2 eV corresponds to the Nb $3d_{3/2}$ photoemission spectra with a spin−orbit splitting of ~2.8 eV, confirming that both signals correspond to Nb^{5+}.[21,22] The Zr 3d spectra are shown in Figure 3c. Two peaks were observed at binding energies of ~182.2 and ~184.6 eV which correspond to $3d_{5/2}$ and $3d_{3/2}$ signals, respectively. Note that these two peaks are separated by a spin−orbit splitting of 2.4 eV, confirming that zirconium is in the form of Zr^{4+}.[21,22] The O 1s photoemission spectra show one signal at 531 eV which can be related to the existence of metal oxides, Figure 4d.

Photoassisted Water Electrolysis. A preliminary, proof-of-concept photoelectrochemical activity test for water photoelectrolysis using the synthesized Ti−Nb−Zr−O nanotube arrays was carried out. Figure 4a shows the photocurrent density versus potential in 1 M KOH solution under UV (320−400 nm, 100 mW/cm^2) illumination for TiO_2 (7 μm long, 21 ± 2 nm wall thickness, annealed at 500 °C, 4 h) and Ti−Nb−Zr−O nanotube array electrodes (4 and 7 μm long, 10 ± 2 nm wall thickness, annealed at 500 °C, 4 h). The photocurrent of the Ti−Nb−Zr−O nanotube samples is slightly higher than that of the pure TiO_2 nanotube sample. The dark current was less than 5 μA/cm^2 for all samples over the displayed potential range. However, the photocurrent onset in the case of Ti−Nb−Zr−O nanotubes occurs at −0.85 V vs Ag/AgCl, a −0.11 V negative shift from that of the TiO_2 nanotube array electrode (−0.74 V), with the slope of the photocurrent−potential curve being higher in the case of Ti−Nb−Zr−O than in the case of TiO_2. Note that this open-circuit voltage represents the contribution of light toward the minimum voltage needed for the water-splitting potential (1.229 V).[7] The current−voltage characteristics of an illuminated semiconductor electrode in contact with a redox electrolyte can be described using the following equation:[3,23]

$$i = i_{ph} - i_0\left[\exp\left(\frac{e_0 V}{kT}\right) - 1\right] \quad (1)$$

where i is the net current obtained by adding the majority and minority current components, i_0 is the reverse bias saturation current, and i_{ph} is the illumination current, which is proportional to the photon flux. The tested nanotube array electrodes show n-type behavior, *i.e.*, positive photocurrents at anodic potentials. For this type of semiconductor, the surface electron density (N_s) decreases with the applied anodic potentials (E_a) as[24]

$$N_s = N_b \exp\left[-e\left(\frac{E_a - V_{fb}}{kT}\right)\right] \quad (2)$$

where N_b is the bulk electron density in the semiconductor, V_{fb} is its flat-band potential, e is the elementary charge, k is Boltzmann's constant, and T is the absolute temperature. Note that $N_s < N_b$ for an n-type semiconductor at all potentials positive of V_{fb}.

For crystalline semiconductors, provided that their absorption coefficient is not too high, the potential dependence of the squared photocurrent (i_{ph}^2) was shown to follow the relation[25]

$$i_{ph}^{\ 2} = \left(\frac{2\varepsilon\varepsilon_0 I^2 \alpha}{N}\right)(V - V_{fb}) \quad (3)$$

where α is the absorption coefficient, V is the applied potential, and V_{fb} is the flat-band potential. Figure 4b shows the squared photocurrent as a function of applied voltage. The current gradually increases, becoming linear with applied bias, indicating that the photogenerated charges are being efficiently separated by the electric field of the depletion layer.[25] At higher potentials, the squared photocurrent−potential plot deviates from linearity due to saturation resulting from the nearly complete collection of photogenerated charge carriers, which is in agreement with literature concerning TiO_2 photoanodes.[8,20] Note that the deviation starts at earlier potentials in the case of Ti−Nb−Zr−O nanotubes than for TiO_2 nanotubes, which might indicate the faster collection of photogenerated charge carriers in the case of Ti−Nb−Zr−O nanotubes. Using linear regression, the linear part of Figure 4b was fitted to eq 3 to estimate the V_{fb} for both TiO_2 and Ti−Nb−Zr−O nanotube films[25] (see Figure S1 in the Supporting Information). It was found that the V_{fb} is −0.575 and −0.451 V for Ti−Nb−Zr−O and TiO_2 nanotube samples, respectively, with corresponding regression coefficients (R) of 0.993 and 0.997.

The corresponding light energy-to-chemical energy conversion (photoconversion) efficiencies are shown in Figure 4c. The photoconversion efficiency η was calculated using the following formula:[2,7]

$$\begin{aligned}\eta\,(\%) &= [(\text{total power output} - \text{electrical power input})/\text{light power input})/] \times 100 \\ &= j_p[(E^0_{rev} - |E_{appl}|)/I_0] \times 100\end{aligned} \quad (4)$$

where j_p is the photocurrent density (in mA/cm^2), $J_pE^0_{rev}$ is the total power output, j_p/E_{appl} is the electrical power input, and I_0 is the power density of incident light (in mW/cm$_2$). E^0_{rev} is the standard reversible potential, which is 1.23 V_{NHE}, and the applied potential $E_{appl} = E_{meas} - E_{aoc}$, where E_{meas} is the electrode potential (versus Ag/AgCl) of the working electrode at which photocurrent was measured under illumination and E_{aoc} is the electrode potential (versus Ag/AgCl) of the same working electrode at open-circuit conditions under the same illumination and in the same electrolyte. Note that eq 4 gives a thermodynamic measure of efficiency which can be applied, in general, to all electrode configurations, *i.e.*, two- or three-electrode cells. However, in the case of a three-electrode configuration, the biased po-

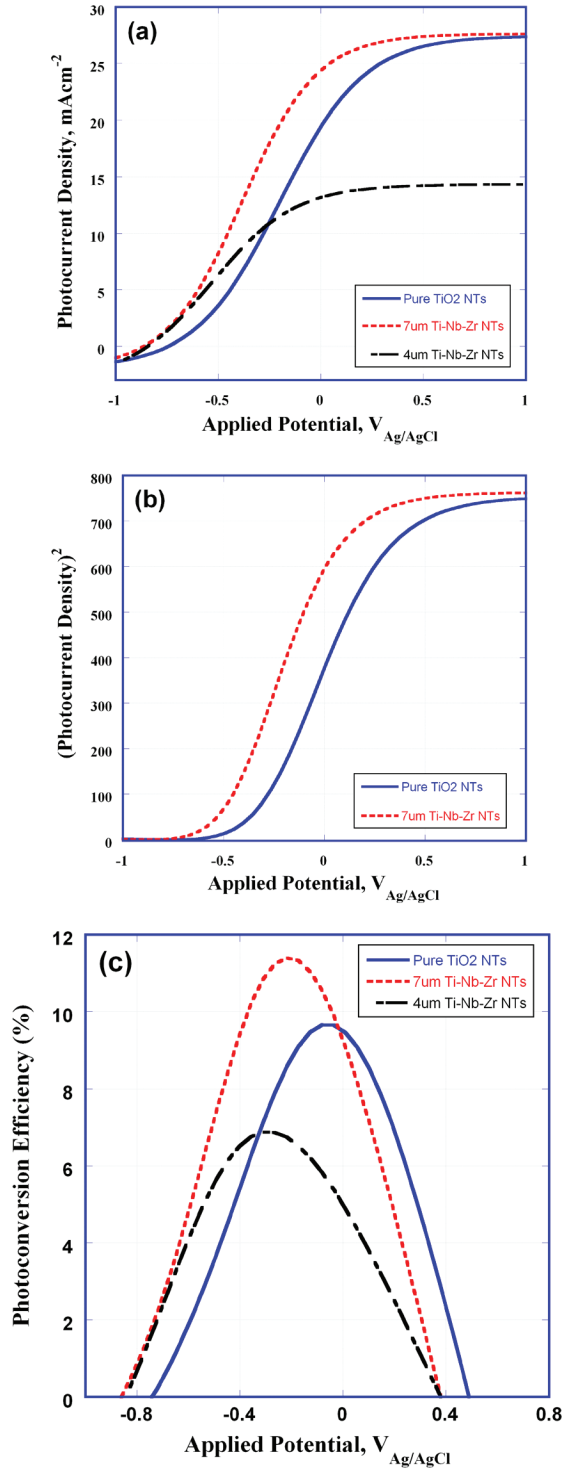

Figure 4. (a) Photocurrent density vs potential in 1 M KOH solution under UV (320−400 nm, 100 mW/cm^2) illumination for TiO_2 (7 μm) and Ti−Nb−Zr−O nanotube (4 and 7 μm) array samples. (b,c) Corresponding squared photocurrent density vs potential and the photoconversion efficiency, respectively.

tential should be measured between the working and counter electrodes.[10] The reference electrode in the three-electrode geometry does not draw any current, and the current flows between the working and counter electrodes.[10] The photoconversion efficiencies for the synthesized nanotube arrays, under 320−400 nm illumination, are ~11.4% for the Ti−Nb−Zr−O nanotubes, 9.7% for the TiO_2 nanotubes having the same length (7 μm), and 6.9% for the 4 μm long Ti−Nb−Zr−O nanotubes. Although the difference in tube length can be used to explain the different photoconversion efficiencies of the 4 and 7 μm long nanotubes, it seems that some other factors come into play when comparing the Ti−Nb−Zr−O and TiO_2 nanotube array photoanodes with the same length (7 μm). The enhanced photoresponse of the Ti−Nb−Zr−O nanotubes sample can be related to the distinct tube structure and composition. For example, the very thin wall thickness of our synthesized Ti−Nb−Zr−O nanotube arrays is expected to play a vital role in such an enhanced photoresponse.[7] The nanotubular architecture, with a wall thickness of 10 ± 2 nm, ensures that the photogenerated holes are never generated far from the semiconductor−electrolyte interface.[7] Furthermore, since half the wall thickness is significantly less than the minority carrier diffusion length (~20 nm in TiO_2),[26] charge-carrier separation takes place efficiently. The potential drop ($\Delta\phi_0$) within the tube wall was shown to follow the relation[8]

$$\Delta\phi_0 = \frac{kTr_0^2}{6eL_D^2} \quad (5)$$

where r_0 is half the width of the wall, T is the temperature, and L_D is the Debye length, given by[8,27]

$$L_D = \left[\frac{\varepsilon\varepsilon_0 kT}{2e^2 N_D}\right]^2 \quad (6)$$

where N_D is the number of ionized donors per cubic centimeter.[27] It is important to note that this potential drop across the wall thickness may not be enough to separate the photogenerated electrons and holes. However, because of the nanoscale dimensions of the walls (10 ± 2 nm), the holes can easily diffuse into the surface, which was shown to takes place on a scale of picoseconds.[27−30] It was also reported that minority carriers generated within a distance from the surface equal to the sum of the depletion layer width and the diffusion length (retrieval length) escape recombination and reach the electrolyte.[31] Note that the relevant dimensional features of our Ti−Nb−Zr−O nanotube arrays (half the wall thickness) are all smaller than 10 nm, which is the range reported for crystalline TiO_2 retrieval length.[28] Therefore, bulk recombination is expected to be reduced and the photoconversion efficiency to be enhanced.[26,28,32,33] This is in agreement with van de Lagemaat and co-workers, who observed a substantial enhancement of the quantum yield in porous SiC made by anodic etching in HF solutions.[34] Note that we have not referred to the effect of surface area on the possibility of surface recombination, as we are comparing two electrodes of almost comparable surface area (TiO_2 and Ti−Nb−Zr−O nanotube arrays 7 μm long each). Another factor that can be considered responsible for the enhanced photoresponse is that the estimated flat-band potential (eq 3) of Ti−Nb−Zr−O photoanode is more favorable than that of the TiO_2 nanotubes photoanode, see Figure S1 (Supporting Information). This is in line with Figure 4c, which shows that the maximum photoconversion efficiency recorded for the Ti−Nb−Zr−O system occurs at lower applied potential than that for the TiO_2 photoanode. One last factor could be that ZrO_2 and Nb_2O_5 are helping slow down charge recombination or inhibit back electron transfer, which can improve the conversion efficiency.[35−37] Similar effects have been noted in Grätzel solar cells by a number of groups.[35−37] That is, the photovoltage and current increase somewhat when TiO_2 is coated by a thin layer of insulating oxide to inhibit back electron transfer from the conduction band (e(cb)) to I_3^-. In our case of photoanodes used to generate oxygen, such a layer could inhibit the back electron transfer between e(cb) and OH radicals near the surface. In this regard, stoichiometric Nb_2O_5 was shown to be an insulator (conductivity (σ) ≈ 3×10^{-6} S cm^{-1})[38] and consequently been used as a porous coating in electrochemical solar cells.[39,40] We note also that Feng and co-workers have coated their TiO_2 nanowire with a layer of Nb_2O_5 to improve the fill factor of their solar cell device. They related the improved efficiency to the ability of the Nb_2O_5 layer to reduce the undesirable recombination processes.[41] Recently, a detailed surface analysis study on Ti−Nb−Zr alloys showed the enrichment of the surfaces of such alloys with Nb and Zr oxide layers upon their thermal oxidation,[42] which supports our claim that these layers can be formed on the nanotube surface (see XPS analysis in Figure 3) and hence held responsible for the observed improved photoconversion efficiency in our system.

CONCLUSIONS

Vertically oriented Ti−Nb−Zr−O nanotube arrays were fabricated *via* the anodization of $Ti_{35}Nb_5Zr$ alloy in aqueous and formamide electrolytes containing NH_4F and H_3PO_4 at room temperature. Similar to pure titanium, the nanotubes fabricated in aqueous electrolytes at 20 V were short in length (1.4 ± 0.4 μm) and contained ridges and circumferential serrations, with no tubular formation observed at anodization potentials lower than 20 V. However, anodization in formamide electrolytes resulted in the formation of well-defined, vertically oriented nanotube arrays with lengths up to 7 μm. These 7 μm long Ti−Nb−Zr−O nanotube arrays showed a three-electrode photoconversion efficiency

of 11.4% under UV illumination (100 mW/cm^2, 320−400 nm, 1 M KOH) upon their use as photoanodes to photoelectrochemically split water, which is about 17.5% higher than that measured for pure TiO_2 of comparable length (9.7%). The thin walls of the Ti−Nb−Zr−O nanotubes (10 ± 2 nm) and the formation of buffering layers (Nb and Zr oxides) are believed to be responsible for the significant conversion efficiency seen with the Ti−Nb−Zr−O samples. Further extended studies are currently being done in our laboratory to establish the validity of these correlations as well as the formulation of any other correlations.

MATERIALS AND METHODS

Prior to anodization, $Ti_{35}Nb_5Zr$ samples (1.0 × 1.0 cm ×0.5 mm) were ultrasonically cleaned with acetone followed by a deionized (DI) water rinse. The anodization was performed in a two-electrode electrochemical cell with the titanium alloy as the working electrode and platinum foil as the counter electrode at room temperature (approximately 24 °C) under the following conditions: (a) in aqueous electrolytes containing 0.2 M NH_4F and 0.1 M H_3PO_4 at 10−20 V for 7 h and (b) in formamide-based electrolytes (ACS grade 99.8% minimum) containing 0.2 M NH_4F, 0.1 M H_3PO_4, and 3 vol % H_2O at 20−40 V for 20 h.[43,44] An Agilent E3612A-CFG001 dc power supply was used for potentiostatic anodization. After anodization, the samples were rinsed thoroughly with DI water and then dried under a stream of nitrogen. The as-anodized samples were crystallized by oxygen annealing for 4 h at 500 °C with a heating and cooling rate of 1 °C/min. The morphology of the anodized samples was examined using a Zeiss SEM Ultra60 field emission scanning electron microscope (FESEM). X-ray photoelectron spectroscopy (XPS) experiments were performed on the Ti−Nb−Zr−O nanotubular films using a Thermo Scientific K-alpha XPS with an Al anode. Spectra were charge-referenced to O 1s at 532 eV. Photoelectrochemical properties were investigated in 1.0 M KOH solution using a three-electrode configuration with nanotube arrays photoanodes, saturated Ag/AgCl as a reference electrode, and platinum foil as a counter electrode. A scanning potentiostat (CH Instruments, model CH 660D) was used to measure dark and illuminated currents at a scan rate of 10 mV/s. A 50 W mercury arc lamp (Exfo lite) was used as the light source, with optical filters used to restrict the incident light to UV wavelengths between 320 and 400 nm.

Acknowledgment. We thank the Department of Energy, grant no. DE-FG02-97ER14799, for support of this work. N.K.A. thanks RAK-CAM Foundation for a postdoctoral fellowship.

Supporting Information Available: Linear regression fitting to calculate the flat-band potential. This material is available free of charge *via* the Internet at http://pubs.acs.org.

REFERENCES AND NOTES

1. Allam, N. K.; Grimes, C. A. Room Temperature One-Step Polyol Synthesis of Anatase TiO_2 Nanotube Arrays: Photoelectrochemical Properties. *Langmuir* **2009**, *25*, 7234–7240.
2. Park, J. H.; Kim, S.; Bard, A. J. Novel Carbon-Doped TiO_2 Nanotube Arrays with High Aspect Ratios for Efficient Solar Water Splitting. *Nano Lett.* **2006**, *6*, 24–28.
3. Allam, N. K.; Shankar, K.; Grimes, C. A. A General Method for the Anodic Formation of Crystalline Metal Oxide Nanotube Arrays without the Use of Thermal Annealing. *Adv. Mater.* **2008**, *20*, 3942.
4. Hassan, F. M. B.; Nanjo, H.; Tetsuka, H.; Kanakubo, M.; Aizawa, T.; Nishioka, M.; Ebina, T.; Bond, A. M. Formation of Self-Ordered TiO_2 Nanotubes by Electrochemical Anodization of Titanium in 2-Propanol/NH_4F. *J. Electrochem. Soc.* **2009**, *156*, K227–K232.
5. Allam, N. K.; Feng, X. J.; Grimes, C. A. Self-Assembled Fabrication of Vertically Oriented Ta_2O_5 Nanotube Arrays, and Membranes Thereof, by One-Step Tantalum Anodization. *Chem. Mater.* **2008**, *20*, 6477–6481.
6. Chen, X.; Mao, S. S. Titanium Dioxide Nanomaterials: Synthesis, Properties, Modifications, and Applications. *Chem. Rev.* **2007**, *107*, 2891–2959.
7. Grimes, C. A.; Varghese, O. K.; Ranjan, S. *Light, Water, Hydrogen: The solar production of hydrogen by water photoelectrolysis*; Springer: Norwell, MA, 2007.
8. Grimes, C. A.; Mor, G. K. *TiO_2 Nanotube Arrays: Synthesis, Properties, and Applications*; Springer: Norwell, MA, 2009.
9. Park, H. G.; Holt, J. K. Recent Advances in Nanoelectrode Architecture for Photochemical Hydrogen Production. *Energy Environ. Sci.* **2010**, *3*, 1028–1036.
10. Murphy, A. B.; Barnes, P. R. F.; Randeniya, L. K.; Plumb, I. C.; Grey, I. E.; Horne, M. D.; Glasscock, J. A. Efficiency of Solar Water Splitting using Semiconductor Electrodes. *Int. J. Hydrogen Energy* **2006**, *31*, 1999–2017.
11. Mor, G. K.; Prakasam, H. E.; Varghese, O. K.; Shankar, K.; Grimes, C. A. Vertically Oriented Ti-Fe-O Nanotube Array Films: Toward a Useful Material Architecture for Solar Spectrum Water Photoelectrolysis. *Nano Lett.* **2007**, *7*, 2356–2364.
12. Mor, G. K.; Varghese, O. K.; Wilke, R. H. T.; Sharma, S.; Shankar, K.; Latempa, T.J.; K.S.; Choi; Grimes, C. A. p-Type Cu-Ti-O Nanotube Arrays and Their Use in Self-Biased Heterojunction Photoelectrochemical Diodes for Hydrogen Generation. *Nano Lett.* **2008**, *8*, 1906–1911.
13. Nah, Y. C.; Ghicov, A.; Kim, D.; Berger, S.; Schmuki, P. TiO_2-WO_3 Composite Nanotubes by Alloy Anodization: Growth and Enhanced Electrochromic Properties. *J. Am. Chem. Soc.* **2008**, *130*, 16154–16155.
14. Bayoumi, F. M.; Ateya, B. G. Formation of Self-organized Titania Nanotubes by Dealloying and Anodic Oxidation. *Electrochem. Commun.* **2006**, *8*, 38–44.
15. Berger, S.; Tsuchiya, H.; Schmuki, P. Transition from Nanopores to Nanotubes: Self-Ordered Anodic Oxide Structures on Titanium-Aluminides. *Chem. Mater.* **2008**, *20*, 3245–3247.
16. Mohapatra, S. K.; Raja, K. S.; Misra, M.; Mahajan, V. K.; Ahmadian, M. Synthesis of Self-organized Mixed Oxide Nanotubes by Sonoelectrochemical Anodization of Ti-8Mn alloy. *Electrochim. Acta* **2007**, *53*, 590–597.
17. Ghicov, A.; Aldabergenova, S.; Tsuchyia, H.; Schmuki, P. TiO_2-Nb_2O_5 Nanotubes with Electrochemically Tunable Morphologies. *Angew. Chem., Int. Ed.* **2006**, *45*, 6993–6996.
18. Ding, D.; Ning, C.; Huang, L.; Jin, F.; Hao, Y.; Bai, S.; Li, Y.; Li, M.; Mao, D. Anodic Fabrication and Bioactivity of Nb-doped TiO_2 Nanotubes. *Nanotechnology* **2009**, *20*, 305103.
19. Yasuda, K.; Schmuki, P. Electrochemical Formation of Self-organized Zirconium Titanate Nanotube Multilayers. *Electrochem. Commun.* **2007**, *9*, 615–619.
20. Allam, N. K.; Shankar, K.; Grimes, C. A. Photoelectrochemical and Water Photoelectrolysis Properties of Ordered TiO_2 Nanotubes Fabricated by Ti Anodization in Fluoride-free HCl Electrolytes. *J. Mat. Chem.* **2008**, *18*, 2341.
21. Biggs, D. *Handbook of X-ray and Ultraviolet Photoelectron Spectroscopy*; Hayden and Son Ltd.: London, 1977.
22. Briggs, D.; Gran, T. J. *Surface Analysis by Auger and X-ray Photoelectron Spectroscopy*; IM Publications: Charlton, Chichester, UK, 2003.
23. Memming, R. *Semiconductor Electrochemistry*; Wiley-VCH, Weinheim, Germany, 2001.
24. Nazeeruddin, M. K.; Kay, A.; Rodicio, I.; Humphry-Baker, R.; Muller, E.; Liska, P.; Vlachopoulos, N.; Gratzel, M.

Conversion of Light to Electricity by cis-X2bis(2,2′-bipyridyl-4,4′-dicarboxylate) Ruthenium(II) Charge-Transfer Sensitizers (X = Cl^-, Br^-, I^-, CN^-, and SCN^-) on Nanocrystalline Titanium Dioxide Electrodes. *J. Am. Chem. Soc.* **1993**, *115*, 6382–6390.
25. Oliva, F.; Avalle, Y. L. B.; Santos, E.; Camara, O. R. Photoelectrochemical Characterization of Nanocrystalline TiO_2 Films on Titanium Substrates. *J. Photochem. Photobiol. A* **2002**, *146*, 175–188.
26. Butterfield, I. M.; Christensen, P. A.; Hamnett, A.; Shaw, K. E.; Walker, G. M.; Walker, S. A. Applied Studies on Immobilized Titanium Dioxide Films as Catalysts for the Photoelectrochemical Detoxification of Water. *J. Appl. Electrochem.* **1997**, *27*, 385–395.
27. Hagfeldt, A.; Gratzel, M. Light-induced Redox Reactions in Nanocrystalline Systems. *Chem. Rev.* **1995**, *95*, 49–68.
28. Sukamto, J. P. H.; Smyrl, W. H.; Mcmillan, C. S.; Kozlowski, M. R. Photoelectrochemical Measurements of Thin Oxide Films: Multiple Internal Reflection Effects. *J. Electrochem. Soc.* **1992**, *139*, 1033–1043.
29. Marin, F. I.; Hamstra, M. A.; Vanmaekelbergh, D. Greatly Enhanced Sub-bandgap Photocurrent in Porous GaP Photoanodes. *J. Electrochem. Soc.* **1996**, *143*, 1137–1142.
30. Vanmaekelbergh, D.; de Jongh, P. E. Driving Force for Electron Transport in Porous Nanostructured Photoelectrodes. *J. Phys. Chem. B* **1999**, *103*, 747–750.
31. Sukamto, J. P. H.; Mcmillan, C. S.; Smyrl, W. Photoelectrochemical Investigations of Thin Metal Oxide Films - TiO_2, Al_2O_3, and HfO_2 on the Parent Metals. *Electrochim. Acta* **1993**, *38*, 15–27.
32. Kopidakis, N.; Benkstein, K.; van de Lagemaat, J.; Frank, A. J. Transport-limited Recombination of Photocarriers in Dye-sensitized Nanocrystalline TiO_2 Solar Cells. *J. Phys. Chem. B* **2003**, *107*, 11307–11315.
33. Benkstein, K. D.; Kopidakis, N.; van de Lagemaat, J.; Frank, A. J. Influence of the Percolation Network Geometry on Electron Transport in Dye-sensitized Titanium Dioxide Solar Cells. *J. Phys. Chem. B* **2003**, *107*, 7759–7767.
34. van de Lagemaat, J.; Plakman, M.; Vanmaekelbergh, D.; Kelly, J. J. Enhancement of the Light to Current Conversion Efficiency in an n-SiC/Solution Diode by Porous Etching. *Appl. Phys. Lett.* **1996**, *69*, 2246–2248.
35. Choi, H.; Kim, S.; Kang, S. O.; Ko, J. J.; Kang, M. S.; Clifford, J. N.; Forneli, A.; Palomares, E.; Nazeeruddin, M. K.; Gratzel, M. Stepwise Cosensitization of Nanocrystalline TiO_2 Films Utilizing Al_2O_3 Layers in Dye-Sensitized Solar Cells. *Angew. Chem., Int. Ed.* **2008**, *47*, 8259–8263.
36. Kay, A.; Gratzel, M. Dye-Sensitized Core-Shell Nanocrystals: Improved Efficiency of Mesoporous Tin Oxide Electrodes Coated with a Thin layer of an Insulating Oxide. *Chem. Mater.* **2002**, *14*, 2930–2935.
37. von Roedern, B. How do Buffer Layers Affect Solar Cell Performance and Solar Cell Stability. *Mater. Res. Soc. Symp. Proc.* **2001**, *668*, H691–H696.
38. Aegerter, M. A. Sol-gel Niobium Pentoxide: A Promising Material for Electrochromic Coatings, Batteries, Nanocrystalline Solar Cells and Catalysis. *Sol. Energy Mater. Sol. Cells* **2001**, *68*, 401–422.
39. Filho, D. D. B.; Franco, D. W.; Filho, P. P. A.; Alves, O. L. Niobia Films: Surface Morphology, Surface Analysis, Photoelectrochemical Properties and Crystallization Process. *J. Mater. Sci.* **1998**, *33*, 2607–2616.
40. Sayama, K.; Sugihara, H.; Arakawa, H. Photoelectrochemical Properties of a Porous Nb_2O_5 Electrode Sensitized by a Ruthenium Dye. *Chem. Mater.* **1998**, *10*, 3825–3832.
41. Feng, X.; Shankar, K.; Varghese, O. K.; Paulose, M.; Latempa, T. J.; Grimes, C. A. Vertically Aligned Single Crystal TiO_2 Nanowire Arrays Grown Directly on Transparent Conducting Oxide Coated Glass: Synthesis Details and Applications. *Nano Lett.* **2008**, *8*, 3781–3786.
42. López, M. F.; Gutiérrez, A.; Jiménez, J. A.; Martinesi, M.; Stio, M.; Treves, C. Thermal Oxidation of Vanadium-Free Ti Alloys: An X-ray Photoelectron Spectroscopy Study. *Mater. Sci. Eng., C* **2010**, *30*, 465–471.
43. Allam, N. K.; Grimes, C. A. Effect of Cathode Material on the Morphology and Photoelectrochemical Properties of Vertically Oriented TiO_2 Nanotube Arrays. *Sol. Energy Mater. Sol. Cells* **2008**, *92*, 1468–1475.
44. Allam, N. K.; El-Sayed, M. A. Photoelectrochemical Water Oxidation Characteristics of Anodically Fabricated TiO_2 Nanotube Arrays: Structural and Optical Properties. *J. Phys. Chem. C* **2010**, *114*, 12024–12029.